

Uncertainty quantification and propagation of errors of the Lennard-Jones 12-6 parameters for n-alkanes

Richard A. Messerly, Thomas A. KnottIV, and W. Vincent Wilding

Citation: [The Journal of Chemical Physics](#) **146**, 194110 (2017); doi: 10.1063/1.4983406

View online: <http://dx.doi.org/10.1063/1.4983406>

View Table of Contents: <http://aip.scitation.org/toc/jcp/146/19>

Published by the [American Institute of Physics](#)

Articles you may be interested in

[Prediction of many-electron wavefunctions using atomic potentials](#)

The Journal of Chemical Physics **146**, 194109 (2017); 10.1063/1.4983395

[Estimating thermodynamic expectations and free energies in expanded ensemble simulations: Systematic variance reduction through conditioning](#)

The Journal of Chemical Physics **146**, 194101 (2017); 10.1063/1.4983164

[Perspective: Dissipative particle dynamics](#)

The Journal of Chemical Physics **146**, 150901 (2017); 10.1063/1.4979514

[Dealing with the exponential wall in electronic structure calculations](#)

The Journal of Chemical Physics **146**, 194107 (2017); 10.1063/1.4983207

[On the accuracy of one- and two-particle solvation entropies](#)

The Journal of Chemical Physics **146**, 194111 (2017); 10.1063/1.4983654

[Nonadditive three-body potential and third to eighth virial coefficients of carbon dioxide](#)

The Journal of Chemical Physics **146**, 054302 (2017); 10.1063/1.4974995



**COMPLETELY
REDESIGNED!**



Physics Today Buyer's Guide
Search with a purpose.

Uncertainty quantification and propagation of errors of the Lennard-Jones 12-6 parameters for *n*-alkanes

Richard A. Messerly,^{a)} Thomas A. Knotts IV, and W. Vincent Wilding
Department of Chemical Engineering, Brigham Young University, Provo, Utah 84602, USA

(Received 9 January 2017; accepted 2 May 2017; published online 19 May 2017)

Molecular simulation has the ability to predict various physical properties that are difficult to obtain experimentally. For example, we implement molecular simulation to predict the critical constants (i.e., critical temperature, critical density, critical pressure, and critical compressibility factor) for large *n*-alkanes that thermally decompose experimentally (as large as C₄₈). Historically, molecular simulation has been viewed as a tool that is limited to providing qualitative insight. One key reason for this perceived weakness in molecular simulation is the difficulty to quantify the uncertainty in the results. This is because molecular simulations have many sources of uncertainty that propagate and are difficult to quantify. We investigate one of the most important sources of uncertainty, namely, the intermolecular force field parameters. Specifically, we quantify the uncertainty in the Lennard-Jones (LJ) 12-6 parameters for the CH₄, CH₃, and CH₂ united-atom interaction sites. We then demonstrate how the uncertainties in the parameters lead to uncertainties in the saturated liquid density and critical constant values obtained from Gibbs Ensemble Monte Carlo simulation. Our results suggest that the uncertainties attributed to the LJ 12-6 parameters are small enough that quantitatively useful estimates of the saturated liquid density and the critical constants can be obtained from molecular simulation. *Published by AIP Publishing.* [<http://dx.doi.org/10.1063/1.4983406>]

I. INTRODUCTION

Accurate estimates for vapor-liquid equilibria, thermo-physical, and transport properties are essential for the efficient design of many chemical processes. When experimental data are not available, these properties are typically estimated with an equation of state (EoS) or empirical prediction model. The critical temperature (T_c), critical pressure (P_c), critical density (ρ_c), and critical compressibility factor (Z_c) of pure compounds are key properties in this regard as the critical constants are often necessary parameters in EoS calculations and in many thermophysical prediction models.^{1–6} The *n*-alkane family is of particular importance due to the significant role it plays in the petrochemical field. However, due to thermal decomposition, experimental critical point data are scarce and potentially unreliable for *n*-alkanes larger than C₁₂. In fact, the existing experimental data demonstrate conflicting trends for T_c and P_c for *n*-alkanes larger than C₁₈.^{7–9} Furthermore, experimental data for ρ_c (and hence Z_c) do not exist for *n*-alkanes larger than C₁₈. In addition, several studies have reported prediction models to extrapolate and/or smooth the existing experimental data. Unfortunately, these prediction models tend to disagree strongly with increasing chain-length.^{7,8,10–15} Molecular simulation presents a possible alternative to the expensive experimental methods and conflicting prediction models.

For example, several studies (including our recent publications) demonstrated how molecular simulation results can help elucidate the correct critical constant trends for long chain-length *n*-alkanes.^{16–21} In a previous study, we performed Gibbs Ensemble Monte Carlo (GEMC) simulations for

compounds as large as hexatetracontane (C₄₈H₉₈) with three different force fields, namely, the Nath, Escobedo, and de Pablo revised force field (NERD),¹⁷ exponential-6 model developed by Errington *et al.* (Exp-6), and Transferable Potentials for Phase Equilibria united-atom (TraPPE-UA).²² Our results were conclusive as to which experimental data, prediction models, and long chain-length trends were most reliable for T_c , P_c , ρ_c , and Z_c .²¹ However, the uncertainties reported in Ref. 21 (and Refs. 16–20 and 22) are strictly statistical uncertainties due to fluctuations in the simulation output and subsequent extrapolation to the critical point. In other words, the uncertainties do not account for possible deficiencies in the force fields themselves.

Since the reliability of molecular simulation results is intimately connected with the intermolecular potential model chosen and the associated model parameters (ϵ , σ , etc.), the model parameters are one of the most important sources of uncertainty. Historically, most studies that report model parameters (i.e., TraPPE-UA,²² NERD,¹⁷ Exp-6,¹⁸ Mie λ -6,²³ Optimized Potentials for Liquid Simulations (OPLS),²⁴ etc.) neglect to perform a statistical analysis of their “best fit” parameters. In 2000, Ray Mountain from the Physical and Chemical Properties Division at the National Institute of Standards and Technology (NIST) detailed a rigorous sensitivity analysis approach and proposed that “sensitivity analysis should be an integral part of potential function/force field development.”²⁵ Despite this endorsement, most simulation studies do not dedicate the effort needed for a useful sensitivity analysis.

Occasionally, the literature provides a sensitivity analysis where the model parameters are varied by an arbitrary amount and the effect on the simulation results is reported.^{26,27} However, a sensitivity analysis of this nature actually

^{a)}Electronic mail: r.alma.messerly@gmail.com

provides little insight because the region of parameter space being sampled usually lands well outside the statistically acceptable range of parameter sets. This is due to two factors. First, the percent that a parameter is varied is often too large to be realistic. Second, the model parameters are correlated since changing one parameter often necessitates a change in another for the parameter set to be statistically acceptable.

A more rigorous approach is to examine what combinations of parameters provide a fit to the data that are acceptable at a given confidence level. Recently, Bayesian statistics have been used for such a purpose.^{28–30} These studies have pioneered the field of force field parameterization uncertainty quantification and propagation of errors (UQ + PoE). Although these studies have focused on small molecules, such as argon and water, their results have been quite promising. In the present study, we employ a more intuitive method of classical (frequentist) statistics UQ + PoE, which NIST classifies as a Type A approach.³¹ In addition, we develop a non-statistical approach to UQ + PoE, referred to by NIST as a Type B approach. This study is significant in that it is the first attempt to quantify the uncertainties due to the intermolecular potential parameters for industrially relevant compounds (*n*-alkanes as large as C₄₈H₉₈).

The primary purpose of this study is four-fold. The first is to develop the Type A (using frequentist statistics) and Type B (using engineering intuition) methodologies of uncertainty quantification in the force field model parameters. Specifically, this analysis will be performed for the Lennard-Jones (LJ) 12-6 parameters (ϵ and σ) for the united-atom (UA) methane (CH₄), methyl (CH₃), and methylene (CH₂) groups. The second purpose is to demonstrate the propagation of errors methodology for properties and compounds not included in the parameterization process. For example, we will quantify how the uncertainties in the CH₃ and CH₂ LJ 12-6 parameters propagate to the critical constants for large *n*-alkanes. The third is to compare the uncertainty quantification and propagation of errors results for the different uncertainty analysis methods. The final purpose is to verify that the uncertainties in the critical constants are small enough to elucidate the correct trends for large *n*-alkanes.

The outline for this document is the following. First, we discuss the approach used to parameterize a transferable potential model. Second, we review the most significant sources of uncertainty in molecular simulations. Third, we develop the Type A and Type B uncertainty quantification and propagation of errors approaches. Then, we apply these analysis methods to quantify the Type A and Type B uncertainties in the CH₃ and CH₂ united-atom Lennard-Jones parameters. Next, we demonstrate how these uncertainties propagate when predicting saturated liquid density (ρ_l , referred to simply as “liquid density” in the remainder of the text), T_c , ρ_c , P_c , and Z_c for *n*-alkanes ranging from C₂–C₄₈. Finally, we discuss some limitations and the primary conclusions of this work.

II. TRANSFERABLE POTENTIAL MODEL FOR *n*-ALKANES

The Transferable Potentials for Phase Equilibria (TraPPE) family of force fields is a popular model with over thirty

transferable LJ 12-6 parameters optimized primarily to predict vapor-liquid coexistence data for organic compounds at industrially relevant state points. In the present study, the term “transferable” simply means that the LJ 12-6 parameters for the CH₃ and CH₂ interaction sites are transferable between *n*-alkane compounds. (It does not imply that the force field can predict all properties at all state points.) The primary objective of transferability is to maximize the ability to build new chemical compounds by minimizing the number of interaction sites included.^{22,25} Because CH₃ and CH₂ sites are commonly found in organic compounds, the *n*-alkane family is a logical starting point for force field parameterization. The united-atom model is implemented because it greatly reduces the number of interaction sites (by grouping hydrogen and carbon atoms into a single site) which enables the simulation of larger molecules that are the primary focus of this study. For these reasons, we have chosen the TraPPE-UA (referred to simply as TraPPE) methodology as our prototype for parameterization. The LJ 12-6 parameter values obtained in this study and their corresponding uncertainties are referred to as the Mess-UP force field (for Messerly *et al.* uncertainty propagation).

In this study, we attempt to replicate the original work done by Martin and Siepmann.²² Specifically, we repeat the TraPPE intermolecular parameterization by performing simulations at the same temperatures, with the same compounds (ethane and *n*-octane), the same model assumptions, and with the same objective function. The objective function used to optimize ϵ_{CH_3} , σ_{CH_3} , ϵ_{CH_2} , and σ_{CH_2} by Martin *et al.* and in this study is

$$RMS(\theta) = \sqrt{\frac{\sum_{i=1}^n (\rho_{li} - \hat{\rho}_l(T_i, \theta))^2}{n}}, \quad (1)$$

where RMS is the root-mean-square, ρ_{li} are the experimental liquid density data at temperature T_i , n is the number of data points, and $\hat{\rho}_l(T_i, \theta)$ is the simulation result for ρ_l at T_i using the force field parameters θ .

Due to limited computational resources at the time (ca. 1998), Martin *et al.* performed four one-dimensional optimizations for the TraPPE *n*-alkane parameters. Specifically, σ was obtained by minimizing RMS for ρ_l and subsequently ϵ was calculated by scaling the vapor-liquid coexistence curve to reproduce the experimental T_c value. Mathematically, this approach is the same as optimizing ϵ and σ simultaneously by minimizing Equation (1) subject to an equality constraint for T_c . However, this is only true if the pair of one-dimensional optimizations is performed iteratively (which was computationally unfeasible for Martin *et al.*) because scaling the vapor-liquid coexistence curve to determine ϵ is not completely rigorous (see note 47 of Ref. 22).

By contrast, in this study, we perform a pair of two-dimensional optimizations where for a given united-atom type, both ϵ and σ are optimized simultaneously by minimizing the RMS in ρ_l . We include T_c as an inequality constraint rather than as an equality constraint as the former is generally preferred in constrained optimization. In other words, we minimize Equation (1) subject to the hard inequality constraint that T_c is predicted to within the experimental and computational uncertainties.

A fundamental assumption in the TraPPE parameterization process is that the ϵ_{CH_3} and σ_{CH_3} values obtained from ethane are transferable to *n*-octane. This assumption greatly simplifies the optimization procedure when compared with regressing all four parameters simultaneously (e.g., NERD,¹⁷ PC-SAFT³²). A four parameter optimization is very difficult primarily due to the strong correlation between the CH_3 and CH_2 parameters.³³ Also, the uncertainty quantification approach outlined in Section IV is considerably more difficult for a four parameter optimization. This is because scanning a 4-dimensional parameter space is more computationally expensive than a pair of 2-dimensional scans. This is another reason why we have chosen the TraPPE model as the prototype in our analysis.

III. SOURCES OF UNCERTAINTY

There are three sources of uncertainty in molecular simulation that are considered the most significant. In general, these uncertainties are classified as numerical, model and parameter uncertainty (although some authors use slightly different distinctions^{28,29}).

The numerical uncertainty refers to the uncertainty in the molecular simulation output due to fluctuations, finite-time, finite-size, simulation parameters, and data analysis methods. In this study, the numerical uncertainty is the uncertainty associated with the vapor-liquid coexistence curve obtained from GEMC simulations and the extrapolation to the critical point. The size of these uncertainties is dependent upon the system size, number of Monte Carlo (MC) cycles, and MC move probabilities³⁴ (provided in Appendix A). Although histogram reweighting Grand Canonical Monte Carlo (GCMC) provides very precise results for vapor phase properties and the critical constants, the precision in ρ_l obtained from GEMC simulations is equal to or superior to that of GCMC.³⁵ Since ρ_l is the only property included in the TraPPE parameterization for *n*-alkanes, we feel that there is little justification for utilizing the GCMC method over the simpler GEMC approach. Furthermore, the critical constants can be predicted from GEMC results with reasonable accuracy, adequate precision, and negligible finite-size effects.^{21,36}

The model uncertainty refers to several different approximations in the force field model. The common sources of model uncertainty are the mathematical form for calculating intramolecular and intermolecular interactions, combining rules of unlike interaction sites, the cutoff length for truncating short and long range interactions, the grouping of an electron cloud into a single point interaction site (either with an all-atom (AA) or united-atom (UA) representation), pair-wise additivity, and the neglect of three body interactions. In this study, the most significant aspects of model uncertainty arise from using the Lennard-Jones 12-6 potential, Lorentz-Berthelot (LB) combining rules, assumption of transferability, and the UA representation. Although we do not explicitly account for model uncertainty, Section VII discusses the possible model limitations.

Finally, parameter uncertainty refers to the imprecision in the force field parameter values. As discussed in Section II, the general approach of parameterization for the

intermolecular LJ 12-6 parameters (ϵ and σ) is to minimize the deviations between simulation results and experimental data of a given physical property (i.e., the objective function). Numerical and model uncertainty tends to increase the minimum value in the objective function and, thus, reduce the precision to which the force field parameters can be known. However, even if the simulation results and the model were exact, there would still be an uncertainty associated with the optimal set of ϵ and σ values. This is because the experimental data have random error (assuming all systematic error has been eliminated by meticulous experimental work). This random error leads to uncertainty in ϵ and σ which leads to uncertainty in any property predicted from the resulting force field. For this reason, an uncertainty quantification and propagation of errors (UQ + PoE) approach is useful when reporting an optimal set of force field parameter values. The remainder of the present work is centered around the UQ + PoE method for the intermolecular LJ 12-6 parameters.

IV. THEORY OF UQ + PoE

Although numerical and model uncertainties can be significant for molecular simulation results, in this work, the discussion will focus on parameter uncertainty. In general, there are two different approaches for estimating uncertainty that are referred to as Type A and Type B in the *Guidelines for Evaluating and Expressing the Uncertainty of NIST Measurement Results*.³¹ A Type A uncertainty analysis utilizes statistical methods while a Type B method employs some other means. Typically a Type A analysis only accounts for random deviations in the experimental data while a Type B analysis also accounts for systematic deviations. A Type B analysis is not as straightforward since it requires an expert evaluation which must consider several factors such as the methodology, the apparatus, the measurement devices, the purity of the sample, the type of data being measured, and the degree of data analysis required. In fact, Cailliez and Pernot recognized systematic deviations and conflicting data as the largest obstacle in UQ of force field models.²⁹ Fortunately, at the Design Institute for Physical Properties (DIPPR 801), this type of analysis is performed by thermodynamic experts that are not only familiar with various experimental methods but also have years of experience in assigning uncertainties. For this reason, we have relied upon the uncertainties reported in the DIPPR 801 database for our Type B analysis.³⁷

Although a Type A and Type B analysis typically refers to uncertainty in data, we use the same terminology for quantifying parameter uncertainty. These terms are useful and appropriate since the parameter uncertainty is primarily a result of the uncertainty in the data used in parameterization. In Secs. IV A–IV B, we present the Type A and Type B UQ + PoE approaches for the specific case of the intermolecular potential parameter uncertainty. Within the Type A framework are two subsets which we call Type A and Type A_B. Type A relies completely upon statistical methods while Type A_B is a hybrid between the two analysis types. After discussing the Type A and Type A_B approaches, we focus on the Type B method.

A. Type A UQ + PoE

The two main approaches for a Type A (statistical) uncertainty quantification analysis are classical (frequentist) and Bayesian. Detailed derivations of the Bayesian approach for molecular simulation can be found in the literature.^{28–30} The frequentist approach is an attractive alternative since it is more intuitive and familiar to most researchers in the molecular simulation field. For this reason, we employ classical frequentist statistics.

1. Parameter uncertainty quantification

In this section, we present a frequentist statistical approach to uncertainty quantification (UQ). The fundamental equation to this method states that³⁸

$$S(\theta) - S(\hat{\theta}) \leq ps^2 F_{p,v,\alpha}, \quad (2)$$

where $S(\theta)$ is the sum squared error of a specific set of parameters (θ), $S(\hat{\theta})$ is the minimized sum squared error of the optimal set of parameters ($\hat{\theta}$), p is the number of parameters, s^2 is an independent estimate of the inherent variance (σ^2) having v degrees of freedom, and $F_{p,v,\alpha}$ is the F-statistic at the α confidence level with p and v degrees of freedom. If a set of parameters, θ , satisfies Equation (2) then the parameter set is acceptable at the $\alpha\%$ confidence level. Note that Equation (2) is compatible with the TraPPE objective function (Equation (1)) since $RMS = \sqrt{\frac{S}{n}}$.

2. Propagation of errors

The uncertainty in ϵ and σ leads to an uncertainty in the simulation results. This propagation of errors (PoE) can be quantified with a standard Monte Carlo sampling (MCS) approach. An important component of an MCS analysis is a means of properly sampling from the p -dimensional parameter space. This is typically done with a probability density function and a random number generator.^{28,29} The probability density function can be obtained by rearranging Equation (2) to obtain

$$PDF(\theta) = F_{p,v}^{-1}\left(\frac{S(\theta) - S(\hat{\theta})}{ps^2}\right), \quad (3)$$

where $PDF(\theta)$ is the probability density function for a specific set of parameters and $F_{p,v}^{-1}$ is the inverse of the F-statistic with p and v degrees of freedom. The PDF is typically displayed as a contour plot where each contour corresponds to a different confidence level.

Before proceeding, it is important to understand the assumptions made in deriving Equation (2) and the possible limitations of this approach. The left-hand side of Equation (2) provides the exact shape of the joint confidence region in the parameters, θ , for both linear and non-linear systems. Furthermore, the fundamental assumption that $\frac{S(\theta) - S(\hat{\theta})}{ps^2}$ follows an F distribution has a strong theoretical basis. However, the “critical values” (i.e., the specific values of $F_{p,v,\alpha}$ and $F_{p,v}^{-1}$) are only approximations. Therefore, the confidence level, α , that satisfies Equation (2) and the PDF values calculated with Equation (3) are approximations to the true confidence level and PDF values, respectively. Fortunately, the F-statistic critical values are an adequate approximation for most systems, especially those that are only moderately non-linear.³⁸

3. Type A and A_B

In order to evaluate Equations (2) and (3), it is necessary to approximate the inherent variance in the data, s^2 . In this study, we have estimated s^2 with both Type A and Type B approaches. (Note that in both cases, the numerical uncertainty in the simulation results can be included in s^2 .) Since the overall methodology is a Type A analysis (i.e., using Equations (2) and (3)), we have distinguished these two approaches as Type A and Type A_B . For a Type A analysis, it is common to assume that

$$s^2 = \frac{S(\hat{\theta})}{n - p} \quad (4)$$

and $v = n - p$. Although s^2 is no longer an independent estimate of σ^2 , it has been shown that this assumption is valid in most practical cases.³⁸ Therefore, in this study, we will perform a Type A analysis using Equations (2)–(4). For the Type A_B analysis, we will still use Equations (2) and (3), but s^2 is approximated from the reported uncertainties in the DIPPR 801 database (u_{DIPPR}).³⁷ Specifically, according to Subsection 4.3 in Ref. 31, we interpret the DIPPR 801 uncertainties as the single measurement 95% confidence interval for a known standard deviation (i.e., $u_{DIPPR} = 1.96 \times \sigma$, the degrees of freedom (v) = ∞ , and, thus, $s^2 = \sigma^2 = \left(\frac{u_{DIPPR}}{1.96}\right)^2$). Since both the Type A and Type A_B analysis methods accept parameter sets based on how they compare with the optimal fit ($S(\hat{\theta})$), they do not consider the possibility of a bias in the data. For this purpose, in Section IV B, we discuss how to account for systematic deviations with a Type B approach.

B. Type B UQ + PoE

The Type B acceptance criterion for a given parameter set depends solely on whether the predicted property values are within the DIPPR 801 uncertainties. The essential difference between the Type A_B and Type B methods is that for temperature dependent properties, the former assigns the DIPPR 801 uncertainties to each data point while the later applies the uncertainties to the entire correlation. Notice that the uncertainties reported by DIPPR 801 are not necessarily uncertainties in the data (s^2), rather they are uncertainties in the correlation. In other words, it is possible that a bias in the data has caused the entire correlation to be shifted one direction. In contrast with both the Type A and Type A_B methods, a Type B analysis can account for a potential bias. Although a Type B approach is not as developed and refined as the Type A (or Type A_B) method, it has some significant practical advantages for molecular simulation. First, it greatly reduces the complexity as well as the computational cost. Second, it may provide a more realistic, conservative, and useful assessment of the reliability of the simulation results.

1. Parameter uncertainty quantification

As the Type B analysis does not have a rigorous statistical derivation, the methodology is much simpler than the Type A approach described previously. A parameter set is considered acceptable (at a pseudo-95% confidence level) if it satisfies the following expression over the desired temperature range:

$$|\hat{y}(T; \theta) - y_{DIPPR}(T)| \leq u_{DIPPR}(T), \quad (5)$$

where $\hat{y}(T; \theta)$ is the predicted property value for the parameter set θ , y_{DIPPR} is the property value from the DIPPR correlation, and u_{DIPPR} is the uncertainty assigned by DIPPR 801. If desired, it is also possible to include the simulation (numerical) uncertainty on the right-hand side of Equation (5).

2. Propagation of errors

Since the Type B approach does not have a rigorous statistical derivation for generating $PDF(\theta)$, we believe that a sufficiently reliable propagation of errors approach is to simply evaluate the predicted property values at the extrema (i.e., corners and edges) of the accepted parameter region. The reason for this assumption is that u_{DIPPR} represents the range in which the “true” value is found 95 out of 100 times, while saying nothing about the distribution of values (analogous to the case described in Subsection 4.6 of Ref. 31). Therefore, since the maximum and minimum values (i.e., $y_{DIPPR} \pm u_{DIPPR}$) correspond to the extrema parameter sets (as demonstrated in Section VI C 1 and Section S.III of the [supplementary material](#)), there is no need to sample from the unknown distribution of interior parameter sets.

C. Comparison of Type A, A_B , and B

The Type B propagation of errors approach has some significant advantages compared to the Type A and A_B methods. For example, the number of molecular simulations and, thereby, the computational costs are reduced significantly by only performing simulations with a few parameter sets at the extrema, rather than sampling hundreds of parameter sets. Furthermore, by contrast with the Type A and Type A_B methods, the Type B approach (Equation (5)) does not require an estimate of the optimal parameter set ($\hat{\theta}$), which is typically a very time consuming and computationally expensive process.

Another advantage of the Type B approach is that it is more compatible with a multi-property optimization than the Type A approach. This is because a Type A approach requires an objective function for calculating the PDF . Multi-property objective functions tend to use complicated and somewhat arbitrary weighting of different data types.³⁹ By contrast, the Type B approach does not require a PDF , which is very tedious and computationally expensive to develop for an entire parameter space. Instead, the multi-property Type B analysis simply requires that the different properties are predicted within their respective uncertainties.

Recently, some simulation studies have attempted to use advanced multi-property methods such as the Pareto front.⁴⁰ We believe that the multi-property Type B approach can reduce the need for an arduous Pareto front analysis while still providing a physically meaningful quantification of uncertainty in molecular simulation results. In Section VI, we demonstrate the ρ_l-T_c multi-property Type B analysis for ethane and *n*-octane.

V. METHODS

A. Type A (and A_B)

The general outlines for the Type A and Type B methodologies are found in Section S.II of the [supplementary](#)

[material](#). The specific steps used in the Type A (and A_B) UQ + PoE analysis for the CH_3 and CH_2 parameters are as follows:

1. Create a 10×14 grid of the 2-dimensional (ϵ by σ) parameter space.
2. Perform GEMC simulations at several temperatures (T_{sim}) for each parameter set.
3. Develop surrogate model from simulation ρ_l values to predict $\hat{\rho}_l(T; \epsilon, \sigma)$.
4. Calculate PDF for a refined parameter grid (500×500).
5. Generate hundreds, thousands, or millions of random numbers.
6. Assign each random number to a parameter set (via the PDF values).
7. Perform GEMC simulations using parameter sets sampled in step 6.
8. Obtain property values for each sampled parameter set.
9. Create histogram of property values obtained in step 8.
10. Integrate histogram (or normal distribution fit) at desired confidence level.

Step 3 is a very useful step for sampling from the parameter space. Essentially, the surrogate model is simply a means of reducing the number of simulations required to calculate the PDF values for the entire parameter space.^{28,41} The surrogate model is used to interpolate between the 10×14 grid of ϵ and σ values that are simulated in step 2. It is also used to interpolate between the simulated temperatures (T_{sim}) so that ρ_l can be predicted at the experimental temperatures (T_{exp}). In addition, the surrogate model assures that the entire parameter space is internally consistent by smoothing out the simulation results. We have provided a detailed validation of the surrogate model in Section S.VI of the [supplementary material](#).

An adequate pseudorandom number generator is an essential aspect to a Monte Carlo sampling propagation of errors approach. The random numbers are used to obtain a properly weighted distribution of parameter sets from the PDF . The amount of random numbers generated in step 5 is determined by the property obtained in step 8. Specifically, if the property has an analytic expression (i.e., a theoretical derivation or surrogate model), it is possible to use on the order of a million random numbers. However, if the property requires performing molecular simulations then the amount of random numbers (parameter sets) generated is limited by the computational costs of step 7.

Steps 9-10 combine the numerical and parameter uncertainties to obtain the overall uncertainty. A PDF of the overall uncertainty is obtained by fitting a normal distribution to the histogram produced in step 9. Since steps 9-10 are important but contribute little to the discussion, we outline the methodology and provide the resultant histograms and uncertainties in Sections S.IV and S.V of the [supplementary material](#).

B. Type B

For the Type B analysis of CH_3 and CH_2 groups, steps 1-3 are the same as those from the Type A and A_B analysis. The remaining steps are as follows:

4. Accept all ϵ and σ parameter sets that satisfy Equation (5).
5. Find extrema of ϵ and σ parameter sets accepted in step 4.
6. Perform GEMC simulations using extrema parameter sets obtained in step 5.
7. Obtain property values and numerical uncertainties for each extrema parameter set.
8. Determine the minimum and maximum property estimates (with numerical uncertainties included).

In step 8, the numerical uncertainty is added to the minimum and maximum property estimates obtained with the extrema parameter sets. Specifically, the overall uncertainty with a Type B analysis is approximated as the lower 95% confidence interval of the minimum estimate and the upper 95% confidence interval of the maximum estimate. Several demonstrations of step 8 are found in Section S.V of the [supplementary material](#).

In summary, we assess the uncertainty in the CH_3 and CH_2 parameters using three different approaches. The first two uncertainties (Type A and A_B) utilize the statistically rigorous Type A analysis approach. The distinction between these two uncertainty types is found in how the inherent uncertainty in the data is approximated, s^2 . Specifically, Type A uncertainties utilize a statistical approach for determining s^2 while Type A_B uncertainties use a Type B approach for assigning s^2 . Note that neither the Type A or A_B uncertainties account for bias in the data, i.e., they assume that the optimal fit of the data is the “best” model. By contrast, the Type B uncertainties account for bias in the data without relying upon a statistically rigorous derivation. In Section VI C, we also demonstrate that the Type B method facilitates the multi-property aspect of obtaining a force field that predicts both ρ_l and T_c to within the DIPPR 801 uncertainties.

VI. RESULTS

An example of the Type A and Type B methodologies and results is found in Section S.III of the [supplementary material](#) for the single-site LJ 12-6 CH_4 molecule. Since the CH_4 group does not contribute to any compounds other than methane, it does not aid in our development of a transferable potential model. The purpose for demonstrating the UQ + PoE approach for the simple case of a UA, LJ 12-6, CH_4 molecule is that the entire parameter space can be scanned analytically. Specifically, the second virial coefficient (B_2), ρ_l , T_c , P_c , and ρ_c can be calculated or estimated without significant computational

costs. This facilitates calculating the *PDF*, generating millions of MCS parameter sets, and propagating the errors in ϵ and σ to B_2 , ρ_l , and the critical constants. By contrast, the parameterization approach utilized for the CH_3 and CH_2 UA sites requires molecule simulations which are much more computationally expensive and are subject to numerical uncertainty, i.e., uncertainty in ρ_l and the critical constants. The following discussion focuses on the UQ + PoE results for the CH_3 and CH_2 LJ 12-6 parameters.

Table I presents the *RMS* values for the optimal CH_3 and CH_2 parameter set obtained in this work (Mess-UP), for the 95% confidence level with the Type A, Type A_B , and Type B uncertainty analysis, and for the TraPPE parameters. There are several key observations from these results. First, the optimal parameter set obtained in this work yields *RMS* values that are nearly an order of magnitude smaller than those of the TraPPE parameter set. For this reason, the Mess-UP parameters are reported with more significant figures. Although our optimal values for ϵ_{CH_3} , σ_{CH_3} , ϵ_{CH_2} , and σ_{CH_2} deviate from those reported by Martin and Siepmann, they are consistent considering the degree of precision with which the TraPPE parameters were reported (two and three significant figures for ϵ and σ , respectively).²² As such, we do not attribute this deviation to the difference in simulation specifications but to the improved precision possible due to advances in computational power. Note that the slightly larger deviation in the CH_2 parameters may be caused by the CH_2 parameters compensating for the small deviation in the CH_3 parameters.

Second, the *RMS* values at the 95% confidence level for both the Type A and Type A_B analysis are smaller than the *RMS* value for the TraPPE parameter set. This suggests that the TraPPE parameter set is statistically different than the Mess-UP optimal parameters. However, it should be noted that the optimal *RMS* reported by Martin *et al.* was approximately the same as the standard deviation in their simulation results. Therefore, with the simulation resources available at the time (ca. 1998), it was not possible to refine the optimal TraPPE parameter values or to obtain more significant figures. Finally, the Type B analysis has the largest *RMS* values which are also larger than the TraPPE *RMS* values. This means that the TraPPE parameter values are acceptable at the 95% confidence level when systematic deviations in the data are considered.

The data used in this study to calculate *RMS* of ρ_l are not identical to the data used by Martin *et al.* The key difference is that this study uses experimental data^{37,42} while Martin *et al.*

TABLE I. Comparison of the root-mean-square (*RMS*, gm/ml) for the optimal parameter set obtained in this work ($\hat{\theta}_{\text{Mess-UP}}$), the 95% confidence level ($\theta, \alpha = 0.95$) for the Type A, Type A_B , and Type B uncertainty analysis, and the TraPPE parameters (θ_{TraPPE}). $\hat{\theta}_{\text{Mess-UP}}$: $\epsilon_{\text{CH}_3} = 98.50$ K, $\sigma_{\text{CH}_3} = 3.749$ Å, $\epsilon_{\text{CH}_2} = 45.38$ K, and $\sigma_{\text{CH}_2} = 3.972$ Å. θ_{TraPPE} : $\epsilon_{\text{CH}_3} = 98$ K, $\sigma_{\text{CH}_3} = 3.75$ Å, $\epsilon_{\text{CH}_2} = 46$ K, and $\sigma_{\text{CH}_2} = 3.95$ Å.

Compound	$RMS(\hat{\theta}_{\text{Mess-UP}})$	$RMS(\theta, \alpha = 0.95)$			$RMS(\theta_{\text{TraPPE}})$	
		Type A	Type A_B	Type B	Martin <i>et al.</i>	This work
Ethane	0.000 29	0.000 39	0.001 72	0.004 73	0.0026	0.0024
<i>n</i> -Octane	0.000 51	0.000 68	0.002 03	0.005 32	0.0044	0.0047

used correlations.⁴³ As different data sets are known to affect the optimal parameter set, a detailed discussion is found in Section S.VII of the [supplementary material](#) to demonstrate that the difference between the two data sets is negligible. Furthermore, to validate this and our previous conclusions, we obtained nearly the same *RMS* value for the TraPPE parameter set as that reported by Martin *et al.* (see Table I). This demonstrates that our methodology, data, and simulation results are consistent with those of Martin *et al.* In addition, this provides a validation of the surrogate model used in this study since the TraPPE parameters were actually not simulated directly, rather the *RMS* values were obtained from the surrogate model.

A. UQ for CH₃ and CH₂

This section presents the uncertainty in the LJ 12-6 parameters for CH₃ and CH₂ UA groups. Figure 1 depicts the 95% confidence regions for the Type A, A_B, and B analysis. For the Type B analysis, we present two acceptable parameter sets (feasible regions). The first predicts ρ_l within the DIPPR uncertainty while the second predicts both ρ_l and T_c to within the DIPPR uncertainties. The extrema points presented in Figure 1 are only those for the Type B analysis with both ρ_l and T_c considered.

There are several key results from Figure 1. The Type B analysis greatly increases the number of acceptable parameter sets because it is no longer assumed that the optimal fit of the data is the “correct” parameter set. Instead, since a bias may exist in the data, it is possible that the “correct” parameter set is one that predicts a consistently lower or higher ρ_l . Furthermore, a parameter set that predicts a ρ_l curve that “cuts through” the experimental data is also considered acceptable as long as the curve remains within the uncertainty bands. For this reason, certain parameter sets predict an acceptable ρ_l curve that extrapolates to an inaccurate T_c value. Therefore, a multi-property optimization appears to be necessary for the Type B analysis to ensure that T_c is also consistent with the experimental value. Recall that this was the original intent of the TrapPE parameterization. That is, Martin *et al.* optimized their parameters such that it would minimize

the deviation in ρ_l while also predicting T_c accurately.²² We did not wish to select a weighting factor in order to develop a multi-property objective function (used for calculating the PDF values) in the Type A (and A_B) analysis. Fortunately, since the Type B analysis uses a cruder uncertainty quantification approach, it is much easier to include additional properties. In addition, the Type A analysis results in such small uncertainties in ρ_l that including T_c (even as a constraint) is unnecessary. Although the Type A_B uncertainties for CH₃ are large enough to result in poor predictions of T_c for ethane, this is not the case for the CH₂ parameters when predicting T_c for *n*-octane.

It is also significant that only a Type B analysis suggests that the TraPPE and NERD CH₂ parameters are acceptable. This is important because with increasing chain-length, the ratio of CH₂ to CH₃ groups increases and the contributions from the CH₃ sites become negligible as only the CH₂ parameter uncertainties should contribute. We can thus conclude, without even performing a Type B PoE analysis (i.e., simulating at the extrema), that the TraPPE and NERD models will predict indistinguishable results for larger *n*-alkanes, i.e., values that lie within the Type B uncertainties. Therefore, the critical constant values that we reported in a previous study for large *n*-alkanes using the TraPPE and NERD model are both acceptable predictions.²¹

Notice that the Type A and A_B confidence regions have an elliptical shape, similar to the results from Cailliez and Pernot,²⁹ while the Type B approach has more linear borders that arise from accounting for bias with a hard constraint (Equation (5)). An elliptical shape that is diagonal signifies that the ϵ and σ parameters are strongly correlated while a rectangular shape parallel to the axis means that the parameters are completely uncorrelated. This observed strong correlation is one reason why it is important to report the joint confidence region for ϵ and σ rather than a pair of single parameter confidence intervals. Finally, it is interesting to notice that the correlation between ϵ and σ is different for the CH₃ parameters than for the CH₂ parameters. We provide a preliminary investigation of this phenomenon in Section S.VI of the [supplementary material](#).

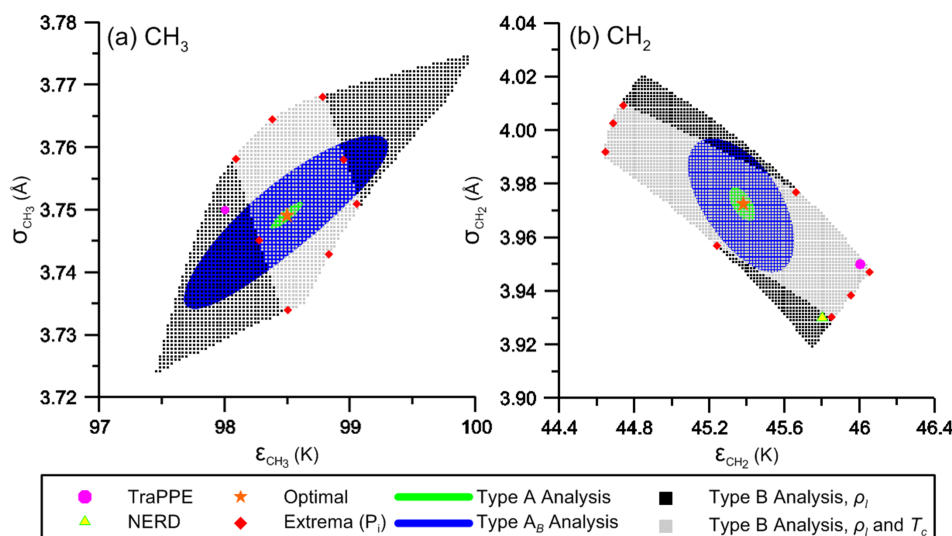


FIG. 1. Comparison of different uncertainty quantification methods. Panels (a) and (b) correspond to the CH₃ and CH₂ LJ parameters, respectively. Each uncertainty analysis region is presented at the 95% confidence level. The extrema parameter sets are those from the Type B analysis when both ρ_l and T_c uncertainties are considered. The TraPPE, NERD, and optimal parameters from this work (Mess-UP) are included as a reference.

B. Sampling of parameter space

This section focuses on the MCS and extrema parameter sets for ϵ and σ . Figure 2 presents the Type A and Type A_B single parameter histograms obtained from millions of random numbers and the respective *PDF* values. Panels (a)-(d) correspond to ϵ_{CH_3} , σ_{CH_3} , ϵ_{CH_2} , and σ_{CH_2} , respectively. From Figure 2 it is clear that the Type A_B single parameter uncertainties are significantly larger than the Type A uncertainties (consistent with Figure 1). Furthermore, the histograms for both uncertainty types and each LJ parameter follow a normal distribution.

Since ϵ and σ are strongly correlated, it is common to create two-dimensional plots of the MCS parameter sets. When the *PDF* contours are also included, these plots can verify that the MCS parameter sets represent a proper sampling from the *PDF*. For example, Figure 3 demonstrates the Type A UQ and MCS results for ϵ_{CH_3} – σ_{CH_3} . The parameter uncertainty (or *PDF*) is presented as contour plots with multiple regions representing different confidence levels. Notice that the contour regions are the 81% (90²%), 90% (\approx 95²%), and 95% confidence levels. Therefore, approximately 5% of the MCS parameter sets should be found beyond the outer confidence

region. Although only 4% of the 2000 MCS parameter sets presented in Figure 3 are outside the 95% confidence region, this is an acceptable result considering the small sample size. Thus, the results from Figure 3 suggest that we have correctly implemented the MCS methodology. Similar plots for the Type A and A_B Monte Carlo sampling of the CH_3 and CH_2 parameters are found in Section S.IV of the [supplementary material](#). These results also suggest that we have correctly implemented the MCS methodology.

When performing a Monte Carlo sampling from the Type A and A_B CH_2 uncertainties for *n*-octane, the CH_3 parameters were set as the optimal parameter set ($\epsilon_{\text{CH}_3} = 98.4966$ and $\sigma_{\text{CH}_3} = 3.7491$). By only sampling from the CH_2 parameter space, we can determine how much the uncertainty in just the CH_2 parameters affects our results for *n*-octane. Since *n*-octane was used in the parameterization process, the PoE results of ρ_l and T_c for *n*-octane can also validate our results for the CH_2 parameters.

Recall that for the Type B analysis, we only simulate the eight extrema points presented in Figure 1. These extrema parameter sets are listed in Table II. Although sampling the eight extrema points for both CH_3 and CH_2 parameter sets would necessitate simulating sixty-four parameter

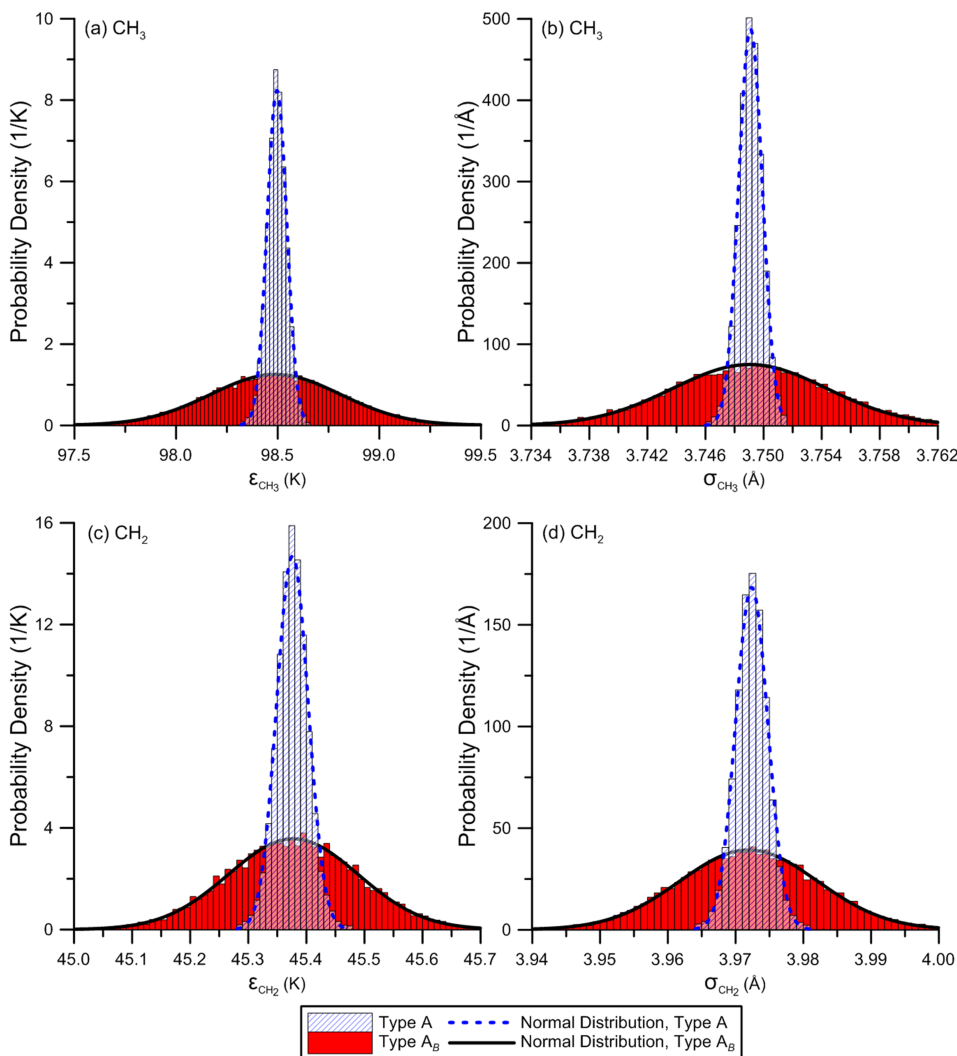


FIG. 2. Histograms of CH_3 and CH_2 LJ parameters from MCS Type A and A_B analysis. Panels (a)-(d) correspond to ϵ_{CH_3} , σ_{CH_3} , ϵ_{CH_2} , and σ_{CH_2} , respectively. The normal distribution fits are also included. Probability density is defined as the number of counts in a single bin divided by both the total number of counts and the bin width.

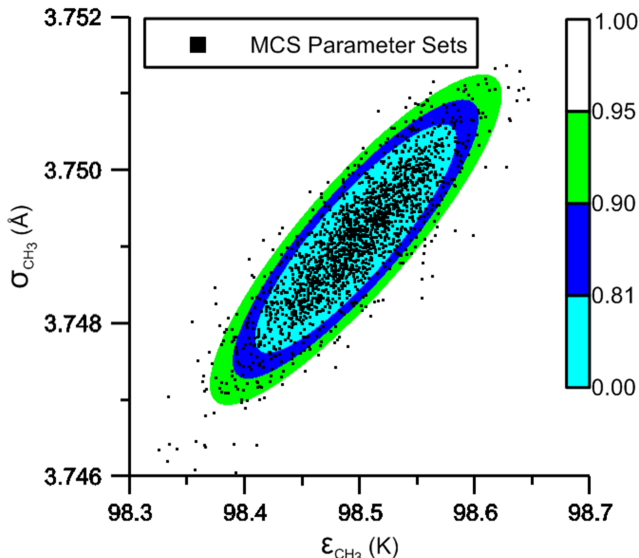


FIG. 3. Contours of the ϵ_{CH_3} – σ_{CH_3} parameters where different color contours correspond to different confidence levels from Type A analysis. The black squares are the Monte Carlo sampling parameter sets that are simulated as part of the propagation of errors.

sets, the CH_3 uncertainty was found to have a negligible effect on the larger n -alkanes. This was verified by simulating C_{16} at the CH_3 extrema points while maintaining the CH_2 parameters at their optimal values (see Figure S.27 of the [supplementary material](#)). Therefore, we only used the optimal CH_3 parameters for C_{16} , C_{24} , C_{36} , and C_{48} to reduce the number of simulations in the Type B analysis. Furthermore, we did not vary the CH_3 parameters for n -octane since we wanted to verify that the Type B uncertainties in ρ_l caused by the CH_2 parameters were the same as the DIPPR uncertainties. Similarly, we used the CH_3 extrema parameter sets in Table II to validate the Type B ρ_l uncertainties for ethane.

C. PoE for CH_3 and CH_2

The uncertainty in the LJ parameters leads to uncertainties in the predicted vapor-liquid coexistence curve and critical point constants. In Subsection VI C 1, we demonstrate the

TABLE II. Extrema parameter sets used in Type B analysis.

P_i	ϵ_{CH_3} (K)	σ_{CH_3} (Å)	ϵ_{CH_2} (K)	σ_{CH_2} (Å)
P_1	98.09	3.758	44.65	3.992
P_2	98.50	3.734	44.74	4.009
P_3	98.78	3.768	45.24	3.957
P_4	99.05	3.751	45.66	3.977
P_5	98.27	3.745	45.85	3.930
P_6	98.95	3.758	46.05	3.947
P_7	98.38	3.765	44.69	4.003
P_8	98.83	3.743	45.95	3.939

Type A, Type A_B , and Type B uncertainties in ρ_l and T_c for ethane and n -octane. These uncertainties are obtained from the propagation of errors method detailed in Section V. We validate that our force field model and parameter uncertainties do in fact match the experimental data values within the stated uncertainties. This discussion focuses on ethane and n -octane as these are the compounds used for optimizing the force field parameters. Finally, we implement the propagation of errors approach for larger compounds. Specifically, we present the uncertainties in ρ_l , T_c , ρ_c , P_c , and Z_c for C_{16} , C_{24} , C_{36} , and C_{48} obtained from the Type A, Type A_B , and Type B analysis. This is done to conclude whether or not the uncertainties in large n -alkanes are small enough to provide quantitative insight.

1. Ethane and n -Octane

In the case of the Type A analysis of ethane, we simulated 2000 MCS sets of ϵ_{CH_3} and σ_{CH_3} . The amount of ϵ and σ values randomly sampled is limited by the computational cost of the system. Fortunately, we did not observe a significant difference between the Type A results obtained with 100 and 2000 parameter sets for ethane (see Section S.IV of the [supplementary material](#)). Therefore, we only used 100 MCS parameter sets for every other system studied with the Type A and A_B analysis in order to significantly reduce the computational cost.

Figure 4 presents the experimental ρ_l data (along with the DIPPR correlation), the values from the TraPPE model, and the results from this work for ethane and n -octane. Notice that the Type A/ A_B results from this work are represented as

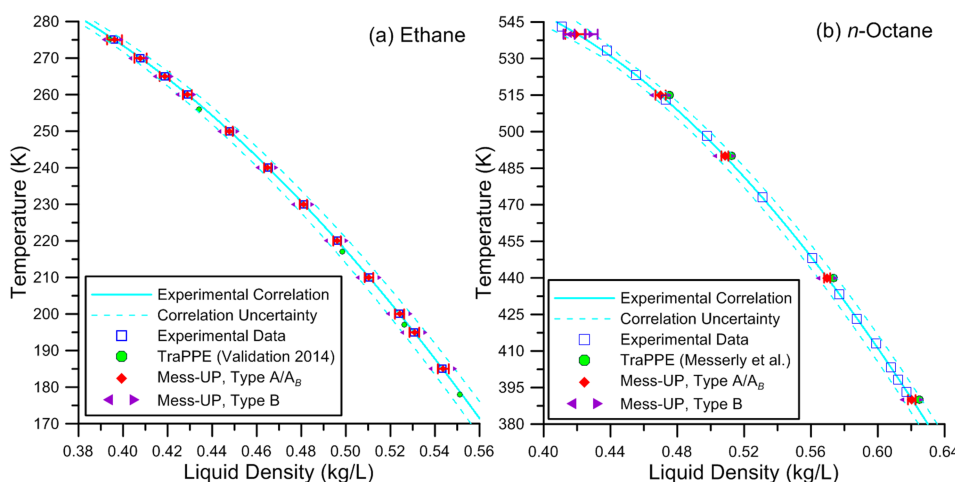


FIG. 4. Comparison of ρ_l experimental data (and a correlation fit to these data) with the TraPPE model and the results from this work. Panels (a) and (b) present results for ethane and n -octane, respectively. The correlation uncertainties are those from the DIPPR 801 database. The error bars represent the 95% confidence interval. The numerical uncertainties for the TraPPE model and the Type B results are approximately one symbol size (except for n -octane at 540 K). Only the uncertainties for the Type A_B analysis are included for the MCS results. The error bars for the Type A analysis are approximately half the size of the Type A_B error bars shown.

a single point at each temperature simulated. These points are the average value obtained from 100 MCS parameter sets. (The average value of 100 MCS parameter sets adequately approximates the value that would be obtained with the optimal parameter set.) The error bars for each data set are reported at the 95% confidence level. The uncertainties for the correlation to the experimental data are those from the DIPPR 801 database (which implements a Type B analysis). The 95% confidence intervals for the TraPPE results are approximately one symbol size. However, the TraPPE uncertainties for ethane and *n*-octane only account for numerical uncertainty as they were obtained from the validation data⁴⁴ and our previous study,²¹ respectively. By contrast, the MCS results presented in this work account for both numerical and parameter uncertainty. For the MCS results, only the error bars for the Type A_B uncertainty analysis are displayed since the error bars for the Type A analysis are less than one symbol size. The Type B results are presented simply as the minimum and maximum ρ_l values obtained from the extrema parameter sets (identified by triangles in Figure 4). The numerical uncertainties in the Type B results are approximately one symbol size (except for *n*-octane at 540 K where the numerical uncertainty is depicted).

There are several key conclusions from Figure 4. First, the Mess-UP model predicts ρ_l very accurately over the entire temperature range. Notice that the TraPPE model has a clear bias (consistently lower for ethane and higher for *n*-octane) when compared with the experimental data and correlation (although it is within the correlation uncertainties). Second, the uncertainty regions obtained from the Type A, Type A_B, and Type B analysis methods vary greatly in magnitude. For example, even the Type A_B uncertainty analysis results in error bars that are still quite small relative to the correlation uncertainty. This demonstrates that uncertainties obtained from strictly statistical means (Type A and A_B) are often smaller than is justifiable. By contrast, the Type B analysis results in ρ_l values that follow the DIPPR correlation uncertainties for the entire temperature range. This validates the assumption that the minimum and maximum values obtained by simulating at the extrema parameter sets adequately reproduce the DIPPR uncertainties. Therefore, we believe that the Type B analysis produces the most meaningful assessment of parameter uncertainty. For this reason, we recommend that future simulation studies utilize the DIPPR 801 uncertainties when performing a UQ + PoE analysis of the force field parameters.

Having demonstrated that our model accurately predicts ρ_l for ethane and *n*-octane, we shift the focus to T_c . Figure 5 presents the PoE results of T_c for ethane and *n*-octane where the uncertainties are presented as probability densities. Figure 5 includes the experimental, TraPPE, Type A, Type A_B, and Type B uncertainties. The experimental uncertainties are obtained by assuming that the DIPPR uncertainties are the 95% confidence interval for a normal distribution of error.³⁷ The TraPPE results only account for numerical uncertainties as the TraPPE validation data were used for ethane⁴⁴ while the results from our previous study were used for *n*-octane.²¹ The TraPPE uncertainties and the numerical uncertainties in our results are obtained from the rigorous nonlinear

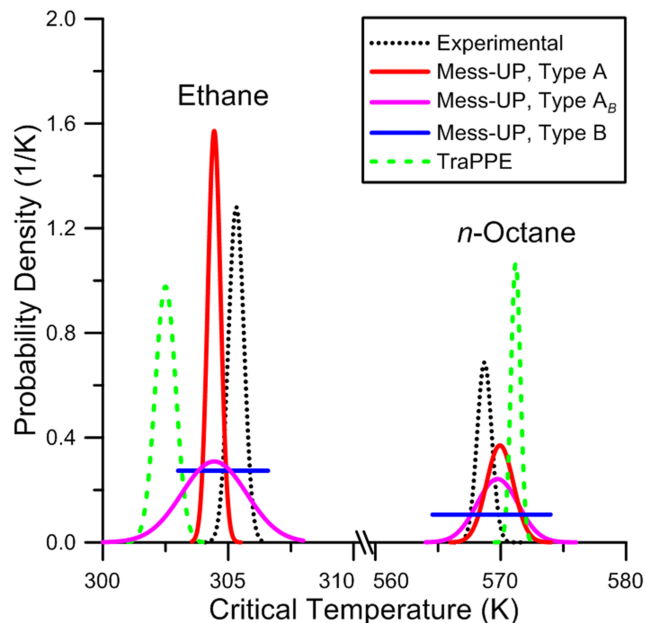


FIG. 5. Comparison of the T_c probability densities (uncertainties) in the experimental data, TraPPE model, and this work for ethane and *n*-octane. The experimental uncertainties are obtained by assuming that the DIPPR uncertainties are the 95% confidence interval for a normal distribution of error.³⁷ The TraPPE uncertainty regions for ethane and *n*-octane are from Refs. 44 and 21, respectively. The Type A and Type A_B results are obtained by fitting a normal distribution to a histogram produced from the 100 MCS parameter sets (2000 in the case of the Type A analysis of ethane). The Type B uncertainty includes the numerical uncertainties of the extrema parameter sets.

analysis methods outlined in our previous work.^{20,45} The Type A and Type A_B uncertainties are obtained by simulating 100 MCS parameter sets and then fitting a histogram of the simulation results to a normal distribution (see Section S.V of the [supplementary material](#)). The Type B results are presented as a region of constant probability ranging from the lowest to the highest values predicted by the extrema parameter sets.

There are several key observations from Figure 5. First, the best estimates (the T_c that corresponds to the peak maximum) for the Mess-UP model are closer to the experimental values than the best estimates for the TraPPE model. In fact, both the Type A and A_B peaks overlap considerably with the experimental peaks. Furthermore, the Type B uncertainty spans the entire experimental uncertainty. This demonstrates that it is sufficient to take the minimum and maximum values from the extrema to represent the Type B uncertainty. The Type B range is slightly wider than the experimental uncertainty region because the Type B range includes the numerical uncertainty (at the 95% confidence level) and the estimated $\pm 0.5\%$ uncertainty attributed to the value of β in the density scaling law (see [Appendix B](#)).^{22,46} Collectively, Figures 4 and 5 demonstrate that the UA, LJ 12-6 model is adequate to predict both ρ_l and T_c to within the given uncertainty for ethane and *n*-octane.

It is also important that the uncertainty in T_c increases only marginally between the Type A and Type A_B analysis for *n*-octane. This suggests that numerical uncertainties are a significant contributor to the overall uncertainty in T_c for larger compounds when obtained from GEMC with the simulation specifications found in [Appendix A](#). This is significant because

the numerical uncertainty for T_c is the smallest of the four critical constants. Therefore, it can be expected that the numerical uncertainties in ρ_c , P_c , and Z_c are larger than their respective parameter uncertainties for the larger n -alkanes. This assumption is validated in Section S.V of the [supplementary material](#).

2. C_{16} , C_{24} , C_{36} , and C_{48}

Figure 6 presents the ρ_l results for C_{16} , C_{24} , C_{36} , and C_{48} . Recall that the Type A and A_B uncertainties were obtained by performing GEMC simulations at 100 CH_3 and CH_2 MCS parameter sets while only the eight CH_2 extrema parameter sets are simulated for the Type B uncertainties. Notice that experimental data are scarce (and have large uncertainties) for these larger compounds in the temperature range considered. For this reason, the DIPPR correlations are provided to help extrapolate the low temperature ρ_l data to which the correlations were fitted (although C_{48} is not included in the DIPPR 801 database). For visual clarity, we have assigned the DIPPR 801 uncertainties to the experimental data rather than to the DIPPR correlations. We have also included “Simulation Correlations” to guide the eye. The “Simulation Correlations” were obtained for the Mess-UP model with the traditional approach of regressing the simulation results to the law of rectilinear diameters and the density scaling law.^{46,47} The TraPPE and NERD results presented in Figure 6 were obtained in a previous study and are considered the most accurate simulations with these models for the compounds in question.²¹ The error bars are the same as those in Figure 4 where the Type A

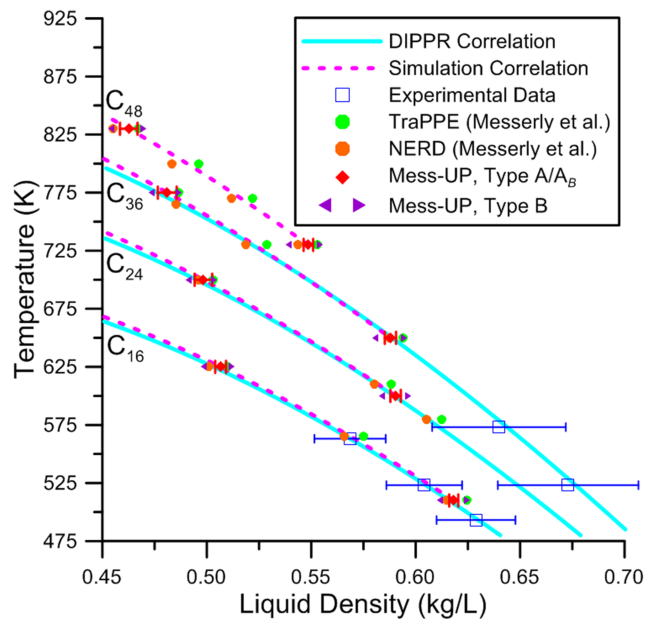


FIG. 6. Comparison of ρ_l experimental data (and a correlation fit to experimental data), the TraPPE and NERD results reported by Messerly *et al.*, and the PoE approach in this work for C_{16} , C_{24} , C_{36} , and C_{48} . The error bars for this work represent the 95% confidence interval for the Type A_B analysis. The DIPPR 801 uncertainties are presented for the experimental data. The error bars for the Type A analysis and the numerical uncertainties for the Type B, TraPPE, and NERD results are approximately one symbol size.

analysis and the numerical uncertainties for the Type B, TraPPE, and NERD results are approximately one symbol size.

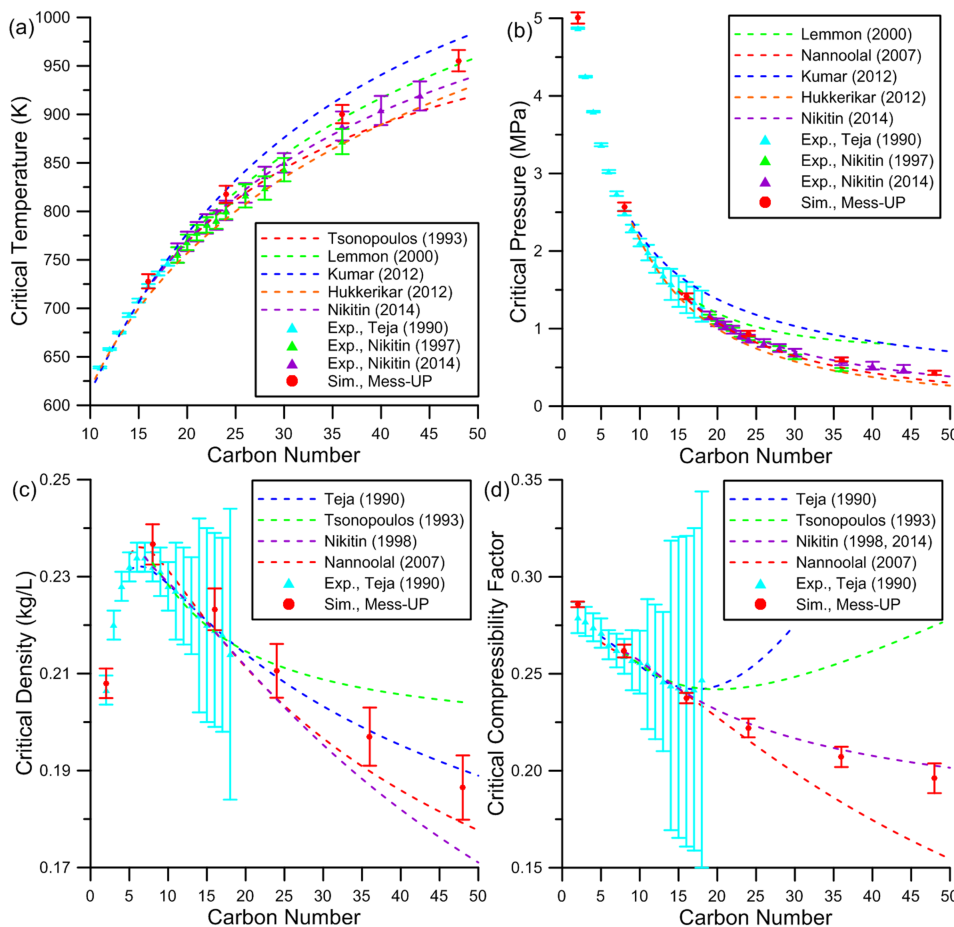


FIG. 7. Comparison of critical constant trends with respect to carbon number for conflicting experimental data, prediction models, and the simulation results from this work. Panels (a)-(d) correspond to T_c , P_c , ρ_c , and Z_c , respectively. Panel (a) excludes smaller n -alkanes because the T_c results for ethane and n -octane were presented previously in Figure 5. The error bars represent the 95% confidence interval. The experimental uncertainties are those from Refs. 8, 9, and 48. The uncertainties for Mess-UP are the largest uncertainty obtained with the Type A, A_B , or B analysis.

We again observe a systematic improvement in the ρ_l values towards the DIPPR 801 correlations when comparing the results for the TraPPE and Mess-UP parameters. Although both the Mess-UP and the TraPPE model agree with the experimental data to within the DIPPR uncertainties, there does appear to be a slight bias in the TraPPE results. As proposed in Section VIA, the Type B lower and upper bounds agree almost identically with the NERD and TraPPE models, respectively. It is significant that the Type B uncertainties are substantially smaller than the DIPPR uncertainties. This suggests that the DIPPR correlations for ρ_l of these larger *n*-alkanes are actually more reliable than DIPPR 801 staff have presumed.

Figure 7 presents the trends for the critical constants T_c , ρ_c , P_c , and Z_c with respect to carbon number. We compare multiple sources of experimental data,^{7–9} several prediction models,^{7,8,10–15} and the Mess-UP simulation results. The uncertainties are reported at the 95% confidence level. Notice that the experimental uncertainties were obtained using a Type B analysis scheme which results in large error bars for certain properties and compounds. Specifically, the Teja T_c , P_c , and ρ_c uncertainties were obtained from a review performed by Ambrose and Tsionopoulos.⁴⁸ The Teja Z_c uncertainties are calculated by assuming that the T_c , P_c , and ρ_c values are uncorrelated. The Nikitin uncertainties are those reported by the authors.^{8,9} In Figure 7, the Mess-UP results represent the average value of 100 MCS parameter sets. The Mess-UP uncertainties represent only the largest overall uncertainty obtained either with the Type A, A_B , and B analysis methods (which is generally that from the Type B analysis). Histograms and PDFs of the Type A, Type A_B , and Type B uncertainties for each compound studied are found in Section S.V of the [supplementary material](#).

The key conclusions from Figure 7 are that the simulation results are reliable enough to elucidate the correct long-chain-length trends even when both the numerical and parameter uncertainties are included. In fact, we arrive at the same conclusions as those in our previous study that only considered numerical uncertainties.²¹ Specifically, the experimental data reported in 2014 by Nikitin *et al.* for T_c and P_c are more reliable than the values originally reported in 1997.^{8,9} P_c does not have an asymptote above 0.5 MPa, ρ_c continues to decrease with increasing carbon number, and Z_c appears to be approaching an asymptote around $\frac{1}{5}$.⁴⁹

VII. LIMITATIONS

Quantifying model uncertainty is difficult, especially when the model is being extrapolated to conditions far removed from the training set used in parameterization. In this study, we have rigorously accounted for numerical and parameter uncertainty without quantifying model uncertainty. Therefore, it is up to the user to determine whether or not the transferable, united-atom (UA), Lorentz-Berthelot (LB), LJ 12-6, pair-wise additive, 14 Å cutoff potential model regressed to ρ_l data is adequate for his/her needs. Generally, the rule of thumb is that the property used to obtain a set of ϵ and σ values should be similar to the property being predicted, i.e., a thermodynamic or transport property and a gas, liquid, or solid phase property. Since we are not concerned with vapor phase and/or transport

properties, we believe that the model uncertainties resulting from the choice of a UA, LB, LJ 12-6 model are negligible. Specifically, we observed in a previous study that TraPPE and NERD (UA, LB, LJ 12-6 force fields) are sufficiently reliable for the purpose of predicting the critical constants of large *n*-alkanes.²¹

One of the largest sources of model uncertainty is due to the inexactness of the mathematical form for intermolecular interactions. It is important to remember that the LJ 12-6 model is only a crude approximation of the true dispersive interactions. Another source of model uncertainty is due to the UA approximation. Although this is often a safe assumption, in some cases, the UA model is known to perform poorly. For example, the TraPPE-EH (explicit hydrogen) model greatly outperforms the TraPPE-UA model for predicting vapor pressure (P_v).⁵⁰ In fact, it has been demonstrated that the UA, LJ 12-6 model is not flexible enough to accurately predict both ρ_l and P_v .²³ The so-called “Pareto” front defines the best compromise obtainable between these competing properties in a multi-property optimization.^{40,51,52} By contrast, the Mess-UP force field is only parameterized to accurately predict ρ_l (and T_c). Therefore, the Mess-UP parameters do not improve the ability of the TraPPE-UA model to predict P_v (see Section S.IX of the [supplementary material](#)). For this reason, it was essential to predict P_c without utilizing P_v (see [Appendix B](#)).

Transferability is another source of model uncertainty. In general, model uncertainties may be a concern when predicting properties for compounds and temperatures not included in the parameterization process. Specifically, the assumption that the CH₃ and CH₂ parameters obtained from ethane and *n*-octane, respectively, transfer to larger *n*-alkanes simulated at higher temperatures may not be valid. In addition, the assumption that the CH₃ parameters transfer from ethane to *n*-octane may cause the optimal CH₂ parameters to compensate and deviate from their “true” values.

A related issue to CH₃ transferability is that the LB combining rules can place a non-physical constraint on the optimal CH₂ parameters. Note that 38% ($\frac{24}{64}$) of the pair-wise interactions for *n*-octane arise from the CH₂–CH₃ cross-interactions. By contrast, the CH₂–CH₃ parameters constitute only 8% ($\frac{184}{2304}$) of the intermolecular interactions for C₄₈. Therefore, it is possible that the “true” CH₂ parameters for *n*-octane are different than the “true” CH₂ parameters for C₄₈. In other words, the assumption of transferability of the CH₃ parameters from ethane and the use of LB combining rules when optimizing the CH₂ parameters from *n*-octane may lead to poor extrapolation for larger *n*-alkanes as the ratio of CH₃ to CH₂ groups decreases relative to *n*-octane.

We believe that the largest potential limitation in the UQ + PoE approach to consider is the correlation between the CH₃ and CH₂ parameter values. In essence, we have assumed that the uncertainty in the CH₃ optimal parameters from ethane is small enough to have a negligible effect on the optimal CH₂ parameters. This assumption reduces the four dimensional parameter space to a pair of independent two dimensional parameter spaces. Therefore, the MCS parameter sets were obtained by independently sampling from the PDFs for the CH₃ and CH₂ parameter spaces. As mentioned previously, Figure S.27 of the [supplementary material](#) demonstrates that the

uncertainty in the CH_3 parameters has a negligible effect on the critical constants for C_{16} . However, the impact of the CH_3 parameter uncertainty on ρ_l for n -octane (which was used in the parameterization process) is likely much larger. Accounting for the correlation between the CH_3 and CH_2 parameters would be greatly simplified if approximate but reliable analytic expressions were developed to relate the CH_2 parameters to the CH_3 parameters. In other words, if the MCS value for σ_{CH_3} deviates from the optimal value, the σ_{CH_2} parameter should likely account for this deviation. Section S.VIII of the [supplementary material](#) presents some preliminary work on this topic.

The intramolecular model is a fundamental (though sometimes overlooked) aspect of any force field. In the present study, we have utilized the TraPPE intramolecular functions and parameters. Therefore, the Mess-UP parameter sets must only be implemented with the TraPPE intramolecular model. In other words, we have assumed that the bond lengths, bond angles, and torsional potential from the TraPPE force field are sufficiently reliable that the effect of their uncertainties on the vapor-liquid coexistence curve is smaller than that of the LJ parameters. For example, although the equilibrium bond angle for smaller n -alkanes may be around 112° , the value of 114° used in the TraPPE model (and in this study) is more reliable for larger n -alkanes, which are the focus of this study. Therefore, we assume that only a small uncertainty is due to deviations in the bond angles for n -octane and larger n -alkanes.

Furthermore, note that Smit *et al.* observed that a different torsional potential resulted in “no significant differences in the phase behavior.”¹⁶ More recently, Bernard-Brunel and Potoff demonstrated that allowing free dihedral rotation had “no effect on the predicted vapor-liquid equilibria” of n -alkanes (along with other compounds).⁵³ However, constraining the n -alkane dihedral angles to only sample from the minimum energy, all *trans* conformation resulted in an observable decrease in saturated liquid density.⁵³ This suggests that substantially different intramolecular models can result in both different optimal LJ parameter sets and uncertainty regions. For this reason, a thorough investigation of the correlation between the C–C bond length in ethane and the optimal ϵ_{CH_3} and σ_{CH_3} parameter sets are found in Section S.X of the [supplementary material](#). The primary conclusion from Section S.X is that the Type B uncertainties in the LJ parameters are sufficiently large to reconcile a wide range of C–C bond lengths.

Three other sources of model uncertainty to consider are the lack of Coulombic interactions, the use of pair-wise additivity, and the long range interaction cutoff distance. It is typically believed that neglecting electrostatic interactions is a safe assumption for n -alkanes. Furthermore, the assumption of pair-wise additivity is typically valid and reasonably accurate. Likewise, a 14 Å long range interaction cutoff with analytic tail-corrections generally leads to a negligible error in the critical constants and in the liquid density at temperatures well below the critical point.^{36,54}

VIII. CONCLUSIONS

In this study, we applied the classical (frequentist) statistical approach of UQ+PoE for the intermolecular

Lennard-Jones 12-6 force field parameters. We also proposed a non-statistical method that relies upon expert evaluation of data to provide a more physically meaningful assessment of parameter uncertainty. The DIPPR 801 database has been particularly useful in this regard. Specifically, we demonstrated how a Type A, Type A_B , and Type B uncertainty analysis can be performed for estimating the uncertainty in the CH_4 , CH_3 , and CH_2 LJ 12-6 parameters. Then, we showed how these uncertainties propagate when predicting ρ_l and the critical constants for large n -alkanes. Somewhat surprisingly, our results demonstrate that the numerical uncertainties (using GEMC) are typically larger or of a comparable magnitude to the Type A and Type A_B parameter uncertainties for T_c , ρ_c , P_c , and Z_c . The Type B parameter uncertainties were much larger but provided a more conservative and feasible estimate of uncertainty in the LJ parameters. Despite these large uncertainties, our results are still conclusive as to which experimental data and prediction models are most reliable for the critical constants of large n -alkanes.

Currently, the most common practice in the literature is to report a single optimal set of force field parameters. Occasionally, some more recent studies have also included the uncertainty for a single parameter (i.e., for ϵ or σ) which provides meaningful quantitative insight.⁵⁵ However, recall that single parameter uncertainties do not account for the correlation that likely exists between the parameters (see Figure 1). With the advances in computational resources and algorithms, we anticipate that more sophisticated and rigorous uncertainty quantification methods be implemented. For example, Refs. 39 and 56 utilize Graphics processing units (GPU) Optimized Monte Carlo (GOMC) to develop “heat maps” that depict a “scoring function.”⁵⁶ This is a great way to visualize the region of acceptable parameter sets. Similarly, Bayesian UQ + PoE studies typically present a Markov chain or posterior sampling that represents feasible parameter sets, analogous to the MCS parameter sets reported in this study.^{28–30}

Rather than reporting a single optimal set of force field parameters, we recommend that future force field development studies report several feasible and acceptable parameter sets (preferably the numerical values). This practice will enable future researchers to approximate the uncertainties in a property of interest as a result of the propagation of errors in the force field parameters. For the Type A and Type A_B approaches, we recommend that at least 100 parameter sets be reported that are obtained from Monte Carlo sampling. For this reason, we have provided lists of MCS parameter sets in Section S.IV of the [supplementary material](#). For the Type B analysis, we believe it is sufficient to report the eight extrema parameter sets as found in Table II. We consider the collective Type A, Type A_B , and Type B ϵ and σ parameter sets as the Mess-UP force field. We encourage future practitioners to avoid utilizing just the optimal parameter sets reported in this study when using the Mess-UP force field.

SUPPLEMENTARY MATERIAL

See [supplementary material](#) for additional information, figures, and data. Section S.I provides an example of determining numerical uncertainties in the critical constants. Section

S.II outlines the general UQ + PoE methodology. Section S.III presents the UQ + PoE results for CH₄. Section S.IV contains the Type A MCS + PoE results for ethane. Section S.V depicts the Type A, A_B, and B histograms (uncertainties) for each compound and physical property. Section S.VI discusses the surrogate model development and validation. Section S.VII is an evaluation of the experimental data used in developing the Mess-UP force field and the correlations used by Martin *et al.* to develop the TraPPE force field. Section S.VIII presents preliminary results for including the correlation between CH₃ and CH₂ parameters. Section S.IX contains the results for P_v of ethane. Section S.X investigates the correlation between the bond length for ethane and the optimal CH₃ parameters.

ACKNOWLEDGMENTS

The authors are grateful to the Design Institute for Physical Properties (DIPPR 801) for funding. They would also like to acknowledge the Brigham Young University Fulton Supercomputing Lab for providing the computational resources to perform thousands of simulations in parallel.

APPENDIX A: SIMULATION SPECIFICATIONS

The simulation specifications are summarized in Table III. As mentioned previously, we have replicated the work originally done to parameterize ϵ_{CH_3} , σ_{CH_3} , ϵ_{CH_2} , and σ_{CH_2} for the TraPPE force field. To be specific, we simulated ethane and *n*-octane at the same temperatures as Martin and Siepmann.²² However, we used more recent simulation protocol to reduce numerical uncertainties,³⁴ i.e., more molecules (N), replicate simulations, and Monte Carlo (MC) cycles for equilibration and production (where an MC cycle consists of N moves). Each MC cycle has a 1%, 13%, 20%, 33%, and 33% probability of performing a volume exchange, molecule

regrowth,⁵⁷ configurational bias exchange,⁵⁸ translation, and rotation move, respectively. All simulations in this study were performed with Gibbs Ensemble Monte Carlo (GEMC) using Towhee.7.0.4 with the DX-1597-2-7 pseudorandom number generator.⁵⁹

Recall that simulations performed for the 10 × 14 grid of ϵ and σ values (step 2 in the Type A and B algorithms presented in Section V) are used for developing the surrogate model to predict $\hat{\rho}_l(T; \epsilon, \sigma)$. The PoE ϵ and σ parameter sets refer to the MCS and extrema parameter sets that are used for propagating the uncertainty in ϵ and σ when estimating the desired properties. The MCS parameter sets are simulated in step 7 of the Type A algorithm while the extrema parameter sets are simulated in step 6 of the Type B algorithm.

Notice that we simulated the PoE parameter sets for ethane at the temperatures that correspond to the experimental data. This was done to validate that our surrogate model predicts ρ_l reliably at the temperatures used in calculating RMS and PDF, i.e., T_{exp} rather than T_{sim} (see Sections S.VI–S.VII of the [supplementary material](#)). In addition, we simulated larger *n*-alkanes at the optimal temperatures for minimizing the numerical uncertainty in the critical constants.^{20,21}

APPENDIX B: DATA ANALYSIS

Estimates for T_c and ρ_c are obtained by regressing the GEMC orthobaric densities to the law of rectilinear diameters⁴⁷ and density scaling law.⁴⁶ The law of rectilinear diameters can be expressed as

$$\rho_r \equiv \frac{\rho_l + \rho_v}{2} = \rho_c + A(T_c - T), \quad (\text{B1})$$

where ρ_r is the rectilinear density, ρ_v is the vapor density, and A is a fitting parameter. The density scaling law is

$$\rho_s \equiv \rho_l - \rho_v = B(T_c - T)^\beta, \quad (\text{B2})$$

TABLE III. Summary of compounds, ϵ and σ parameter sets, total number of molecules (N), temperatures (T_{sim}), number of replicates at each temperature (n_r), and the number of Monte Carlo cycles in the equilibration (MC_E) and production (MC_P) periods.

Compound	ϵ and σ	N	T_{sim} (K)	n_r	MC_E	MC_P
Ethane (C ₂ H ₆)	10 × 14 grid	800	178, 197, 217, 236, 256, 275	12	20 000	80 000
Ethane (C ₂ H ₆)	PoE	800	185, 195, 200, 210, 220, 230, 240, 250, 260, 265, 270, 275	2	20 000	80 000
<i>n</i> -Octane (C ₈ H ₁₈)	10 × 14 grid	400	390, 440, 490, 515, 540	9	20 000	80 000
<i>n</i> -Octane (C ₈ H ₁₈)	PoE	400	390, 440, 490, 515, 540	6	20 000	80 000
<i>n</i> -Hexadecane (C ₁₆ H ₃₄)	PoE	200	510, 625	10	40 000	160 000
<i>n</i> -Tetracosane (C ₂₄ H ₅₀)	PoE	200	600, 700	10	40 000	160 000
<i>n</i> -Hexatriacontane (C ₃₆ H ₇₄)	PoE	200	650, 775	10	40 000	160 000
<i>n</i> -Octatetracontane (C ₄₈ H ₉₈)	PoE	200	730, 830	10	40 000	160 000

where ρ_s is the scaling density, B is a fitting parameter, and β is a constant, typically 0.326.³⁶ (Although a value of 0.326 was used for ethane to be consistent with the TraPPE validation data, a value of 0.32 was used for *n*-octane to be consistent with the work of Martin and Siepmann.) The estimate for P_c is calculated according to the Vetere method by rearranging the Rackett equation^{20,60} as

$$P_c = \frac{R_g T_c \rho_c}{M_w} \left(\frac{\rho_c}{\rho_l} \right)^{\left(1 - \frac{T_l}{T_c}\right)^{-\gamma}}, \quad (\text{B3})$$

where R_g is the universal gas constant, M_w is the molecular weight, T_l is the temperature corresponding to ρ_l , and γ is an empirical parameter estimated to be $\frac{2}{7}$. The critical compressibility factor is defined as

$$Z_c \equiv \frac{P_c M_w}{R_g T_c \rho_c}. \quad (\text{B4})$$

As demonstrated in our previous studies, by using Equation (B3), it is possible to obtain reliable estimates of P_c from united-atom Lennard-Jones based force fields (TraPPE, NERD).^{20,21} This is important since these force fields (and the Mess-UP force field developed in this study) are not capable of predicting vapor pressure (P_v) to the accuracy required to utilize the traditional approach of extrapolating P_v to the critical point with the Antoine equation.²⁰

Finally, the numerical uncertainties in T_c , ρ_c , P_c , and Z_c are obtained using the nonlinear statistical analysis explained in our previous studies.^{20,45} The numerical uncertainties in the critical constants are expressed as probability densities. The numerical uncertainties account for the scatter in the simulation output and the regression using Equations (B1) and (B2). Since these numerical uncertainties are utilized in the Type B analysis, Section S.I of the supplementary material provides an example for the TraPPE-UA ethane validation data.⁴⁴

Systematic errors caused by limitations of Equations (B1)–(B3) are more difficult to quantify. In our previous studies, we demonstrated that uncertainties in β and γ are smaller than the numerical uncertainties for P_c and Z_c .^{20,21} However, systematic errors for T_c resulting from β are estimated to be $\pm 0.5\%$.²² Therefore, T_c uncertainties of less than this value are not justified. As only the Type A uncertainty for T_c of ethane is less than $\pm 0.5\%$, in general, the uncertainty in β is negligible compared to the uncertainties in the force field parameters.

- ¹V. L. Bhirud, "Saturated liquid densities of normal fluids," *AIChE J.* **24**(6), 1127–1131 (1978).
- ²C. F. Chueh and A. C. Swanson, "Estimating liquid heat-capacity," *Chem. Eng. Prog.* **69**(7), 83–85 (1973).
- ³B. I. Lee and M. G. Kesler, "Generalized thermodynamic correlation based on 3-parameter corresponding states," *AIChE J.* **21**(3), 510–527 (1975).
- ⁴J. W. Przezdziecki and T. Sridhar, "Prediction of liquid viscosities," *AIChE J.* **31**(2), 333–335 (1985).
- ⁵S. R. S. Sastri and K. K. Rao, "A new temperature-thermal conductivity relationship for predicting saturated liquid thermal conductivity," *Chem. Eng. J.* **74**(3), 161–169 (1999).
- ⁶C. Tsionopoulos, "Empirical correlation of second virial-coefficients," *AIChE J.* **20**(2), 263–272 (1974).
- ⁷A. S. Teja, R. J. Lee, D. Rosenthal, and M. Anselme, "Correlation of the critical properties of alkanes and alkanols," *Fluid Phase Equilib.* **56**, 153–169 (1990).

- ⁸E. D. Nikitin and A. P. Popov, "Critical temperatures and pressures of C₄₀, C₄₄, and C₆₀ normal alkanes measured by the pulse-heating technique," *Fluid Phase Equilib.* **379**, 191–195 (2014).
- ⁹E. D. Nikitin, P. A. Pavlov, and A. P. Popov, "Vapour-liquid critical temperatures and pressures of normal alkanes with from 19 to 36 carbon atoms, naphthalene and *m*-terphenyl determined by the pulse-heating technique," *Fluid Phase Equilib.* **141**(1-2), 155–164 (1997).
- ¹⁰E. W. Lemmon and A. R. H. Goodwin, "Critical properties and vapor pressure equation for alkanes C_nH_{2n+2}: Normal alkanes with n <= 36 and isomers for n = 4 through n = 9," *J. Phys. Chem. Ref. Data* **29**(1), 1–39 (2000).
- ¹¹C. Tsionopoulos and Z. M. Tan, "The critical constants of normal alkanes from methane to polyethylene: II. Application of the Flory theory," *Fluid Phase Equilib.* **83**, 127–138 (1993).
- ¹²A. Kumar and R. Okuno, "Critical parameters optimized for accurate phase behavior modeling for heavy *n*-alkanes up to C₁₀₀ using the Peng-Robinson equation of state," *Fluid Phase Equilib.* **335**, 46–59 (2012).
- ¹³Y. Nannoolal, J. Rarey, and D. Ramjugernath, "Estimation of pure component properties: Part 2. Estimation of critical property data by group contribution," *Fluid Phase Equilib.* **252**(1-2), 1–27 (2007).
- ¹⁴A. S. Hukkerikar, B. Sarup, A. T. Kate, J. Abildskov, G. Sin, and R. Gani, "Group-contribution⁺ (GC⁺) based estimation of properties of pure components: Improved property estimation and uncertainty analysis," *Fluid Phase Equilib.* **321**, 25–43 (2012).
- ¹⁵E. D. Nikitin, "The critical properties of thermally unstable substances: Measurement methods, some results and correlations," *High Temp.* **36**(2), 305–318 (1998).
- ¹⁶B. Smit, S. Karaborni, and J. I. Siepmann, "Computer-simulations of vapor-liquid phase-equilibria of *n*-alkanes," *J. Chem. Phys.* **102**(5), 2126–2140 (1995).
- ¹⁷S. K. Nath, F. A. Escobedo, and J. J. de Pablo, "On the simulation of vapor-liquid equilibria for alkanes," *J. Chem. Phys.* **108**(23), 9905–9911 (1998).
- ¹⁸J. R. Errington and A. Z. Panagiotopoulos, "A new intermolecular potential model for the *n*-alkane homologous series," *J. Phys. Chem. B* **103**(30), 6314–6322 (1999).
- ¹⁹E. A. Muller and A. Mejia, "Comparison of united-atom potentials for the simulation of vapor-liquid equilibria and interfacial properties of long-chain *n*-alkanes up to *n*-C₁₀₀," *J. Phys. Chem. B* **115**(44), 12822–12834 (2011).
- ²⁰R. A. Messerly, T. A. Knotts, R. L. Rowley, and W. V. Wilding, "An improved approach for predicting the critical constants of large molecules with Gibbs ensemble Monte Carlo simulation," *Fluid Phase Equilib.* **425**, 432–442 (2016).
- ²¹R. A. Messerly, T. A. Knotts IV, R.L. Rowley, and W. V. Wilding, "Improved estimates of the critical point constants for large *n*-alkanes using Gibbs ensemble Monte Carlo simulations," *J. Chem. Eng. Data* **61**(10), 3640–3649 (2016).
- ²²M. G. Martin and J. I. Siepmann, "Transferable potentials for phase equilibria. 1. United-atom description of *n*-alkanes," *J. Phys. Chem. B* **102**(14), 2569–2577 (1998).
- ²³J. J. Potoff and D. A. Bernard-Brunel, "Mie potentials for phase equilibria calculations: Applications to alkanes and perfluoroalkanes," *J. Phys. Chem. B* **113**(44), 14725–14731 (2009).
- ²⁴W. L. Jorgensen, J. D. Madura, and C. J. Swenson, "Optimized intermolecular potential functions for liquid hydrocarbons," *J. Am. Chem. Soc.* **106**(22), 6638–6646 (1984).
- ²⁵J. C. Rainwater, D. G. Friend, H. J. M. Hanley, A. H. Harvey, C. D. Holcomb, A. Laesecke, J. W. Magee, and C. Muzny, Report on forum 2000: Fluid properties for new technologies - connecting virtual design with physical reality, National Institute of Standards and Technology Special Publication 975, pp. 100–112, 2000.
- ²⁶J. Chang and S. I. Sandler, "Interatomic Lennard-Jones potentials of linear and branched alkanes calibrated by Gibbs ensemble simulations for vapor-liquid equilibria," *J. Chem. Phys.* **121**(15), 7474–7483 (2004).
- ²⁷A. Tsourtis, Y. Pantazis, M. A. Katsoulakis, and V. Harmandaris, "Parametric sensitivity analysis for stochastic molecular systems using information theoretic metrics," *J. Chem. Phys.* **143**(1), 014116 (2015).
- ²⁸P. Angelikopoulos, C. Papadimitriou, and P. Koumoutsakos, "Bayesian uncertainty quantification and propagation in molecular dynamics simulations: A high performance computing framework," *J. Chem. Phys.* **137**(14), 144103 (2012).
- ²⁹F. Cailliez and P. Pernot, "Statistical approaches to forcefield calibration and prediction uncertainty in molecular simulation," *J. Chem. Phys.* **134**(5), 054124 (2011).

- ³⁰F. Rizzi, H. N. Najm, B. J. Debusschere, K. Sargsyan, M. Salloum, H. Adalsteinsson, and O. M. Knio, "Uncertainty quantification in MD simulations. Part II: Bayesian inference of force-field parameters," *Multiscale Model. Simul.* **10**(4), 1460–1492 (2012).
- ³¹B. N. Taylor and C. E. Kuyatt, "NIST guidelines for evaluating and expressing the uncertainty of NIST measurement results cover," NIST Technical Note 1297, pp. 1–9, 1994.
- ³²T. van Westen, T. J. H. Vlugt, and J. Gross, "Determining force field parameters using a physically based equation of state," *J. Phys. Chem. B* **115**(24), 7872–7880 (2011).
- ³³S. Ueyigitler, M. C. Camurdan, and J. Richard Elliott, "Optimization of transferable site-site potentials using a combination of stochastic and gradient search algorithms," *Ind. Eng. Chem. Res.* **51**(17), 6219–6231 (2012).
- ³⁴A. D. C. Morales, I. G. Economou, C. J. Peters, and J. I. Siepmann, "Influence of simulation protocols on the efficiency of Gibbs ensemble Monte Carlo simulations," *Mol. Simul.* **39**(14–15), 1135–1142 (2013).
- ³⁵A. S. Paluch, V. K. Shen, and J. R. Errington, "Comparing the use of Gibbs ensemble and grand-canonical transition-matrix Monte Carlo methods to determine phase equilibria," *Ind. Eng. Chem. Res.* **47**(13), 4533–4541 (2008).
- ³⁶M. Dinpajoo, P. Bai, D. A. Allan, and J. I. Siepmann, "Accurate and precise determination of critical properties from Gibbs ensemble Monte Carlo simulations," *J. Chem. Phys.* **143**(11), 114113 (2015).
- ³⁷R. L. Rowley, W. V. Wilding, J. L. Oscarson, T. A. Knotts, and N. F. Giles, "DIPPR data compilation of pure chemical properties," in *Design Institute for Physical Properties* (AIChE, New York, NY, 2013).
- ³⁸E. M. L. Beale, "Confidence regions in non-linear estimation," *J. R. Stat. Soc. Ser. B* **22**(1), 41–88 (1960).
- ³⁹J. R. Mick, "Force field development with GOMC, a fast new Monte Carlo molecular simulation code," Ph.D. thesis, Wayne State University, 2016.
- ⁴⁰K. Stöbener, P. Klein, S. Reiser, M. Horsch, K.-H. Küfer, and H. Hasse, "Multicriteria optimization of molecular force fields by Pareto approach," *Fluid Phase Equilib.* **373**, 100–108 (2014).
- ⁴¹M. Hulsmann and D. Reith, "SpaGrOW—A derivative-free optimization scheme for intermolecular force field parameters based on sparse grid methods," *Entropy* **15**(9), 3640 (2013).
- ⁴²M. Funke, R. Kleinrahm, and W. Wagner, "Measurement and correlation of the (P, ρ , T) relation of ethane II. Saturated-liquid and saturated-vapour densities and vapour pressures along the entire coexistence curve," *J. Chem. Thermodyn.* **34**(12), 2017–2039 (2002).
- ⁴³B. D. Smith and R. Srivastava, *Thermodynamic Data for Pure Compounds. Part A. Hydrocarbons and Ketones* (Elsevier, Amsterdam, New York, 1986), Distributors for the U.S. and Canada E.
- ⁴⁴B. L. Eggemann, P. Bai, A. P. Bliss, Q. P. Chen, T. F. Chen, A. D. Corest-Morales, E. Fetisov, E. Haldoupis, D. B. Harwood, R. K. Lindsey, T. L. Arachchi, M. S. Shah, H. D. Stern, K. N. Struk, J. Sung, A. J. Sunnarborg, B. Xue, and J. I. Siepmann, T-UA No. 2 Ethane, TrapPE Validation Database, University of Minnesota, Minneapolis, MN, <http://www.chem.umn.edu/groups/siepmann/trappe/>, accessed 2015 June 11.
- ⁴⁵R. A. Messerly, R. L. Rowley, T. A. Knotts, and W. V. Wilding, "An improved statistical analysis for predicting the critical temperature and critical density with Gibbs ensemble Monte Carlo simulation," *J. Chem. Phys.* **143**(10), 104101 (2015).
- ⁴⁶J. S. Rowlinson, *Liquids and Liquid Mixtures*, Butterworths Monographs in Chemistry, 3rd ed. (Butterworth Scientific, London, Boston, 1982).
- ⁴⁷A. C. Biswas, "The law of rectilinear diameter for the liquid-gas phase transition," *Pramana* **1**(2), 109–111 (1973).
- ⁴⁸D. Ambrose and C. Tsionopoulos, "Vapor-liquid critical properties of elements and compounds. 2. Normal alkanes," *J. Chem. Eng. Data* **40**(3), 531–546 (1995).
- ⁴⁹J. C. Pamies and L. F. Vega, "Critical properties of homopolymer fluids studied by a Lennard-Jones statistical associating fluid theory," *Mol. Phys.* **100**(15), 2519–2529 (2002).
- ⁵⁰B. Chen and J. I. Siepmann, "Transferable potentials for phase equilibria. 3. Explicit-hydrogen description of normal alkanes," *J. Phys. Chem. B* **103**(25), 5370–5379 (1999).
- ⁵¹S. Werth, K. Stöbener, P. Klein, K.-H. Küfer, M. Horsch, and H. Hasse, "Molecular modelling and simulation of the surface tension of real quadrupolar fluids," *Chem. Eng. Sci.* **121**, 110–117 (2015), Danckwerts Special Issue on Molecular Modelling in Chemical Engineering, 2013.
- ⁵²K. Stöbener, P. Klein, M. Horsch, K. Küfer, and H. Hasse, "Parametrization of two-center Lennard-Jones plus point-quadrupole force field models by multicriteria optimization," *Fluid Phase Equilib.* **411**, 33–42 (2016).
- ⁵³D. A. Bernard-Brunel and J. J. Potoff, "Effect of torsional potential on the predicted phase behavior of *n*-alkanes," *Fluid Phase Equilib.* **279**(2), 100–104 (2009).
- ⁵⁴N. M. Fischer, P. J. van Maaren, J. C. Ditz, A. Yildirim, and D. van der Spoel, "Properties of organic liquids when simulated with long-range Lennard-Jones interactions," *J. Chem. Theory Comput.* **11**(7), 2938–2944 (2015).
- ⁵⁵P. Bai, M. Tsapatsis, and J. Ilja Siepmann, "TrapPE-zeo: Transferable potentials for phase equilibria force field for all-silica zeolites," *J. Phys. Chem. C* **117**(46), 24375–24387 (2013).
- ⁵⁶J. R. Mick, M. S. Barhagi, B. Jackman, K. Rushaidat, L. Schwiebert, and J. J. Potoff, "Optimized Mie potentials for phase equilibria: Application to noble gases and their mixtures with *n*-alkanes," *J. Chem. Phys.* **143**(11), 114504 (2015).
- ⁵⁷J. I. Siepmann and D. Frenkel, "Configurational bias Monte-Carlo—A new sampling scheme for flexible chains," *Mol. Phys.* **75**(1), 59–70 (1992).
- ⁵⁸C. D. Wick and J. I. Siepmann, "Self-adapting fixed-end-point configurational-bias Monte Carlo method for the regrowth of interior segments of chain molecules with strong intramolecular interactions," *Macromolecules* **33**(19), 7207–7218 (2000).
- ⁵⁹M. G. Martin, MCCCS Towhee, <http://towhee.sourceforge.net/>.
- ⁶⁰H. G. Rackett, "Equation of state for saturated liquids," *J. Chem. Eng. Data* **15**(4), 514–517 (1970).